

Bound excited states of Fröhlich polarons in one dimension

J. Taylor,^{1,2,3,4} M. Čufar,^{1,2} D. Mitrouskas,⁵ R. Seiringer,⁵ E. Pahl,^{3,4} and J. Brand^{1,2,*}

¹Dodd-Walls Centre for Photonic and Quantum Technologies, Auckland 0745, New Zealand

²Centre for Theoretical Chemistry and Physics, New Zealand Institute for Advanced Study, Massey University, Private Bag 102904, North Shore, Auckland 0745, New Zealand

³MacDiarmid Institute for Advanced Materials and Nanotechnology, Auckland 1010, New Zealand

⁴Department of Physics, University of Auckland, Auckland 1010, New Zealand

⁵Institute of Science and Technology Austria (ISTA), Am Campus 1, 3400 Klosterneuburg, Austria

(Dated: June 3, 2025)

The one-dimensional Fröhlich model describing the motion of a single electron interacting with optical phonons is a paradigmatic model of quantum many-body physics. We predict the existence of an arbitrarily large number of bound excited states in the strong coupling limit and calculate their excitation energies. Numerical simulations of a discretized model demonstrate the complete amelioration of the projector Monte Carlo sign problem by walker annihilation in an infinite Hilbert space. They reveal the threshold for the occurrence of the first bound excited states at a value of $\alpha \approx 1.73$ for the dimensionless coupling constant. This puts the threshold into the regime of intermediate interaction strength. We calculate the spectral weight and the number density of the dressing cloud in the discretized model.

Studies of the polaron, describing the motion of an electron in a polarizable medium, go back almost a century to the works of Landau [1] and Pekar [2]. Formalised by Fröhlich [3], the polaron model is one of the most studied problems of quantum many-body theory [4] with real-world relevance for electronic material properties [5]. Calculations of the ground state energy, the dispersion relation and also the structure of the excitation continuum have been achieved at great accuracy and become an important test bed for analytical [6] and numerical [7–10] techniques. Thus it may seem surprising that evidence for bound excited states below the excitation continuum has emerged only very recently [11].

The proof of the existence of arbitrarily many bound excited states in the strong-coupling limit of the three-dimensional model [11] demonstrates that previous approaches have missed key features of the Fröhlich polaron at intermediate and strong coupling. Previous numerical studies have failed to produce evidence for bound excited states in the three-dimensional case [8]. Studies of one-dimensional Fröhlich polaron models found excitations of the electron as resonances at high energies within the phonon continuum [12, 13]. In contrast, for the Holstein model of a small polaron, the existence of a bound excited state below the continuum is well known [14–16].

In this Letter we calculate the energies of the bound excited states of the phonon dressing cloud for the Fröhlich model in one dimension in the strong coupling limit, and provide numerical evidence for them in the weak to intermediate coupling regime applying Full Configuration Interaction Quantum Monte Carlo (FCIQMC) [17–19]. The first bound excited state appears at $\alpha \approx 1.73$, which is in a crossover regime between weak and intermediate coupling strength with a spectral weight of ≈ 0.2 , suggesting that these states may be accessible in experiments.

FCIQMC is a modern flavor of Projector Quantum Monte Carlo [20]. Originally developed for electronic structure calculations of molecules [17], it has been extended to bosonic

systems [21, 22] and electron-phonon systems with infinite Hilbert space [23]. Sampling the ground and excited [19, 24] states of the Fröhlich model in Fock space provides us with direct access to the energies and properties of these states, avoiding the ill-conditioned analytic continuation procedure required to obtain spectral information from diagrammatic Monte Carlo calculations [8]. Our state-of-the art semi-stochastic [18, 25] implementation of FCIQMC [26, 27] allows us to sample ground and excited states with moderate stochastic error and well-controlled systematic biases. Specifically, we report the first successful amelioration of the sign problem in Projector Monte Carlo [28] by walker annihilation in an infinite Hilbert space without employing sign-problem-mitigating approximations. Previously, this was only achieved in calculations with a finite Hilbert space [17, 29–31].

The model – The one-dimensional Fröhlich model describes an electron interacting with lattice vibrations in one dimension. The original three-dimensional Fröhlich Hamiltonian [3] was generalized to arbitrary dimensions in Refs. [32, 33]. The Hamiltonian in the one-dimensional case is

$$\hat{H} = \frac{\hat{p}^2}{2m} + \hbar\omega_{\text{LO}} \sum_k \hat{a}_k^\dagger \hat{a}_k - \hbar\omega_{\text{LO}} \sqrt{\frac{2\alpha}{L/l_0}} \sum_k \left(\hat{a}_k e^{ik\hat{r}} + \hat{a}_k^\dagger e^{-ik\hat{r}} \right), \quad (1)$$

where \hat{p} and \hat{r} are the electron momentum and position, \hat{a}_k^\dagger and \hat{a}_k are the phonon creation and annihilation operators, ω_{LO} is the frequency of longitudinal optical phonons (taken to be constant), m is the band mass of the electron, and α is a dimensionless coupling constant. L is the length of the system with periodic boundaries (eventually taken to be infinite), and $l_0 = \sqrt{\hbar/2m\omega_{\text{LO}}}$ is a natural unit of length.

The energy-momentum spectrum consists of an isolated ground state band [34] with decreasing energy as the coupling strength increases, and a continuum of scattering states starting at an energy of $1\hbar\omega_{\text{LO}}$ above the ground state [35]. Al-

though the absence of discrete excited states can be proven at weak coupling [36], discrete (bound) excited states with energies below the continuum exist at intermediate and strong coupling, as will be shown in the following.

Excitation energies in the strong coupling limit – For large α , the discrete excited eigenvalues of \hat{H} in Eq. (1) at total momentum $P = 0$ can be obtained analytically, and are given by

$$\frac{E_j}{\hbar\omega_{\text{LO}}} \approx -\frac{\alpha^2}{3} - \frac{1}{2} \sum_{i \geq 0} (1 - \omega_i) + \omega_j, \quad j = 0, 1, \dots \quad (2)$$

As is well-known [37–39], the first term, $-\alpha^2/3$, represents the semiclassical energy obtained by minimizing the corresponding Pekar functional with respect to the electron wave function $\psi(x)$ and the classical polarization field $\phi(x)$. The Pekar functional (given in dimensionless units integrating over $x = r/l_0$)

$$\mathcal{E}^P[\psi, \varphi] = \int |\psi'|^2 - 2\sqrt{2\alpha} \int |\psi|^2 \text{Re}(\varphi) + \int |\varphi|^2 \quad (3)$$

is obtained as an expectation value of the Hamiltonian of Eq. (1) with respect to a product of the electron wave function $\psi(x)$ and a coherent state for the phonon field with amplitude $\varphi(x)$. The physical picture is that, at large coupling, the polarization field effectively becomes classical, and the electron occupies the ground state in the corresponding effective potential. The Pekar functional has the explicit minimizer $\psi^P(x) = \sqrt{\alpha/2} \text{sech}(\alpha x)$ for the electron wave function and $\varphi^P(x) = \sqrt{2\alpha}\psi^P(x)^2$ for the polarization field. The other terms in Eq. (2) involving the (α independent) frequencies ω_j quantify the quantum fluctuations of the field around its classical value [11, 40–44]. Letting the electron take the instantaneous ground state in a varying field, they are obtained by expanding $\min_{\psi} \mathcal{E}^P[\psi, \varphi^P + \varphi]$ to second order in $\varphi(x)$, with the result

$$-\frac{\alpha^2}{3} + \|\text{Im}(\varphi)\|^2 + \langle \text{Re}(\varphi), \hat{\omega}^2 \text{Re}(\varphi) \rangle. \quad (4)$$

Here the Hessian operator takes the simple form

$$\hat{\omega}^2 = 1 + 8\alpha\partial\psi^P(-\partial^2 + \alpha^2)^{-2}\psi^P\partial, \quad (5)$$

where $\psi^P(x)$ is understood as a multiplication operator, and $\partial = d/dx$. By scaling, the eigenvalues of $\hat{\omega}$ are independent of α . We denote them by $0 = \omega_0 < \omega_1 \leq \dots < 1$. There is a single zero mode, $\omega_0 = 0$, resulting from translation invariance. The lowest non-vanishing eigenvalues are given by $\omega_1 \approx 0.647$ and $\omega_2 = \sqrt{7/9} \approx 0.882$. For details, we refer to Appendix A in the End Matter.

We proceed by quantizing the field $\varphi(x) \rightarrow \hat{\varphi}(x)$. Expanding $\hat{\varphi}(x) = \sum_{j \geq 0} \hat{c}_j u_j(x)$ in terms of the (real-valued) eigenfunctions $u_j(x)$ of $\hat{\omega}^2$, and defining $\hat{p}_j = \sqrt{2}\text{Im}(\hat{c}_j)$ and $\hat{q}_j = \sqrt{2}\text{Re}(\hat{c}_j)$, we re-interpret the quadratic terms in Eq. (4) as a sum of harmonic oscillators with frequencies ω_j :

$$\frac{1}{2} \sum_{j \geq 0} (\hat{p}_j^2 + \omega_j^2 \hat{q}_j^2). \quad (6)$$

This leads to a contribution to the ground state energy of the form $\frac{1}{2} \sum_{j \geq 0} \omega_j = \infty$ from the zero-point motion. To obtain the finite quantum corrections, we need to subtract the (infinite) energy of the fluctuations in the absence of the electron, however, leading to the corrected expression $\frac{1}{2} \sum_{j \geq 0} (\omega_j - 1)$, hence justifying Eq. (2) for $j = 0$. Numerically, one finds $\frac{1}{2} \sum_{j \geq 0} (\omega_j - 1) \approx -0.95$. For $j \geq 1$, the excitation energies correspond to excitations of different oscillators in Eq. (6). Since $\omega_j > \frac{1}{2}$ for $j \geq 1$, only single excitations can appear below the continuum. The zero mode $j = 0$ needs to be discarded for the calculation of the excitation spectrum of Eq. (1) due to the restriction to zero total momentum.

Lee-Low-Pines transformation – Using a unitary transformation due to Lee, Low, and Pines amounting to a frame transformation [45], the electron coordinate dependence of the Fröhlich polaron Hamiltonian of Eq. (1) can be eliminated and the Hamiltonian rewritten in terms of the conserved total momentum P :

$$\hat{H}_{\text{LLP}} = \frac{1}{2m} \left(P - \hbar \sum_k \hat{k} \hat{a}_k^\dagger \hat{a}_k \right)^2 + \hbar\omega_{\text{LO}} \sum_k \hat{a}_k^\dagger \hat{a}_k - \hbar\omega_{\text{LO}} \sqrt{\frac{2\alpha}{L/l_0}} \sum_k (\hat{a}_k^\dagger + \hat{a}_k). \quad (7)$$

This equivalent Hamiltonian acts only on a Fock space of phonons for a given value of the total momentum P and is more convenient for numerical calculations. We take the system size L finite, which discretizes the phonon modes with the values of k restricted to multiples of $2\pi/L$. A finite number of modes M used in numerical calculations results in a momentum cutoff of $k_c = \pi(M-1)/L$. Even so, the phonon Hilbert space dimension is still formally (and practically) infinite, as an arbitrary number of phonons can reside in each mode. Technically, the number of phonons in each mode is limited to be < 256 by the 8-bit number type used for representing the Fock basis. We perform calculations with up to $M = 73$ and Hilbert space dimension $256^M \approx 6 \times 10^{175}$. In the following, we will restrict the analysis to $P = 0$.

FCIQMC – The algorithm samples the ground state of \hat{H}_{LLP} by repeatedly applying the operator $1 - d\tau(\hat{H}_{\text{LLP}} - S)$ to a coefficient vector. The shift parameter S is updated to keep the norm (the number of ‘walkers’) approximately constant [21], and therefore provides an estimator of the eigenstate energy after equilibration. The operation is performed exactly for coefficients with a modulus above a given threshold and stochastically for the rest. Combined with stochastic vector compression [46], this implements a semistochastic algorithm, where part of the Hamiltonian matrix is treated deterministically while the rest is sampled stochastically [18, 25]. Crucially, contributions of opposite sign to a coefficient can annihilate and thus reduce sign noise. At sufficiently large walker number, the sign of the dominant coefficients becomes stable by a spontaneous symmetry-breaking process [28, 47] and the sign problem is mitigated. The residual noise leads to stochastic errors and also causes a small population control

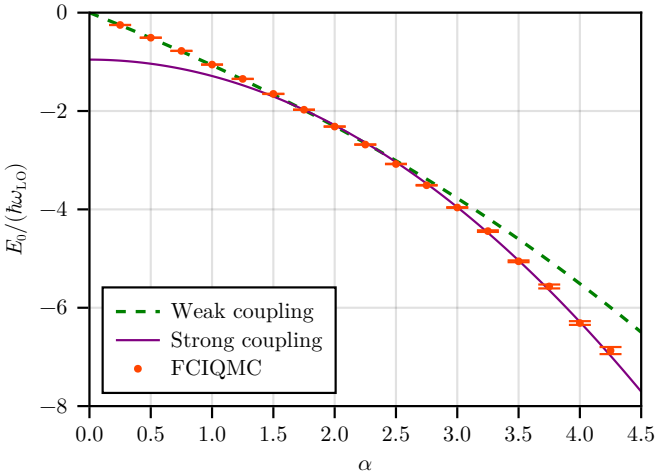


FIG. 1. The ground state energy E_0 of the one-dimensional Fröhlich polaron, calculated using FCIQMC for various coupling strengths, compared with theoretical expansions in the weak [Eq. (8)] and strong coupling [Eq. (9)] regimes. The FCIQMC calculations used $L = 6l_0$ and $k_c = 12\pi/l_0$.

bias [22, 48, 49], which we control by increasing the walker number until undetectable levels of the bias are seen that are smaller than the stochastic error bars.

If both the box size L and the momentum cutoff k_c are large enough, the results obtained using the discretized model approach the continuum limit. We find that the energies converge exponentially in L , but only algebraically in k_c (see Supplemental Material [50]).

Ground state energy – In the weak coupling limit, the ground state energy has been found analytically using perturbation theory [33, 51] and the path integral formalism [52]. For $P = 0$, the ground state energy is

$$\frac{E_0}{\hbar\omega_{\text{LO}}} \approx -\alpha - 0.06066\alpha^2 - 0.00844\alpha^3 + \mathcal{O}(\alpha^4). \quad (8)$$

While the numerical prefactors were rounded, this is exact to third order in α . In the strong coupling limit, the ground state energy of Eq. (2) evaluates to

$$\frac{E_0}{\hbar\omega_{\text{LO}}} \approx -\frac{\alpha^2}{3} - 0.955 + \mathcal{O}(\alpha^{-2}). \quad (9)$$

Figure 1 shows the transition from the weak coupling regime, through an intermediate coupling regime around $\alpha \approx 2$ where both expansions approximately overlap, into the strong coupling regime as the coupling strength α increases. While there is no phase transition separating the weak and strong coupling regimes, different physical pictures apply [53]. Our FCIQMC approach allows us to probe both regimes and the transition region comfortably. At $\alpha = 2$ we estimate the discretization error to be around 1% and about an order of magnitude larger than the stochastic error [50].

Excited state energies – In order to calculate excited states numerically with FCIQMC, the computation is initialized

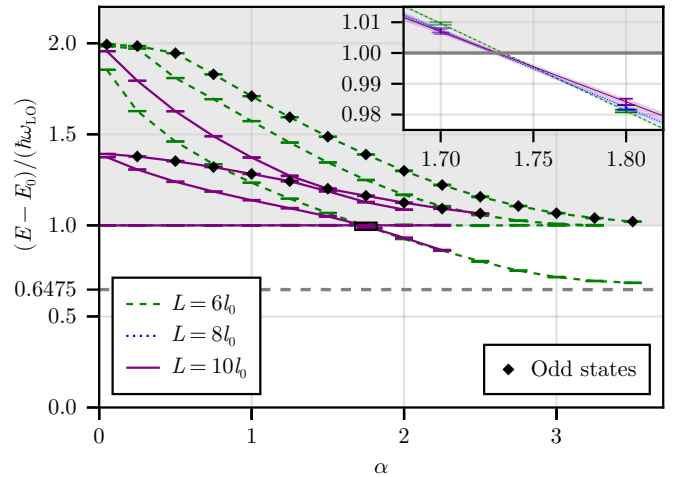


FIG. 2. The excitation energies of the first four excited states, with zero total momentum, calculated using FCIQMC for various coupling strengths and box sizes (error bars and symbols). The first bound excited state appears at $\alpha \approx 1.73$, in the intermediate coupling regime. The dashed horizontal line corresponds to the analytical result for the first discrete excitation energy at large α . The shaded region shows the phonon continuum for $L \rightarrow \infty$. All states other than those labeled as odd are even under a parity transformation. Energies for $L = 8l_0$ are only shown in the inset.

with multiple starting vectors, which are then orthogonalized at every step (or a specified number of steps) of the computation using the Gram-Schmidt procedure. This ensures that the n^{th} vector converges to the n^{th} eigenvector, and the n^{th} shift acts as an estimator for the n^{th} -lowest eigenvalue [19].

Even though the ground state calculation with the Hamiltonian (7) is free of the Monte Carlo sign problem, excited state calculations introduce the sign problem [28, 29] due to the necessary existence of nodes in the excited state wave functions [19]. The sign problem manifests itself at low walker number in fluctuating signs of all state vector coefficients and an average value of the shift $\langle S \rangle$ that is lower than the correct energy [17, 31]. Increasing the walker number above a critical value, the shift average stabilizes and becomes independent of the walker number, indicating that the sign problem is overcome. For the studied range of α values we find that 10^7 walkers is sufficient, indicating that the sign problem is relatively weak in this case [31]. This is remarkable as the unconstrained phonon occupation makes the Hilbert space of the Fröhlich Hamiltonian (7) infinite. For details, see Appendix B in the End Matter.

Figure 2 shows the excitation energies of a few low-lying excited states as function of α and for different box sizes L at $P = 0$. At the bottom of the phonon continuum (shaded region) there is always one state with an excitation energy of $1\hbar\omega_{\text{LO}}$. It is given by $|\text{C}\rangle = (\hat{a}_0^\dagger - \sqrt{2\alpha l_0/L})|\text{GS}\rangle$, where $|\text{GS}\rangle$ denotes the ground state. For weak coupling this is the first excited state in the spectrum. Due to the finite box size, the continuum of eigenstates with excitation energies above $1\hbar\omega_{\text{LO}}$ is discretized. This discretization is most easily under-

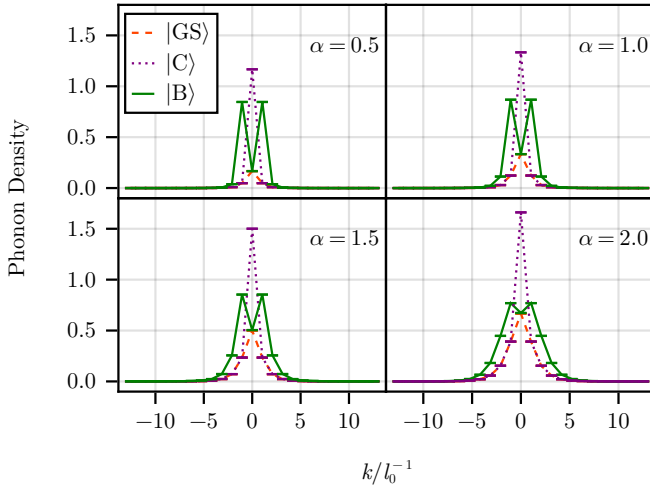


FIG. 3. The density of virtual phonons in each mode $\langle j | a_k^\dagger a_k | j \rangle$ for the ground state $|j\rangle = |\text{GS}\rangle$ and first two excited states, with $L = 6l_0$ and $k_c = 4\pi/l_0$, for various coupling strengths. The state $|\text{C}\rangle$ is at the start of the continuum, and always has an excitation energy of $\hbar\omega_{\text{LO}}$. The state $|\text{B}\rangle$ is a bound excited state for $\alpha \gtrsim 1.73$.

stood for vanishing coupling strength $\alpha = 0$. In this case, the Hamiltonian is diagonal in the Fock state basis with eigenvalues $E_{a,b}/\hbar\omega_{\text{LO}} = a + (2\pi b l_0/L)^2$, where $a \in \mathbb{N}$ is the total number of phonons, and $b \in \mathbb{Z}$ is the total phonon momentum in units of $\frac{2\pi\hbar}{L}$. As the coupling strength α increases, some of the excitation energies decrease.

As seen in Fig. 2, the first bound state with excitation energy below $1\hbar\omega_{\text{LO}}$ appears at $\alpha \approx 1.73$, in the intermediate coupling regime. While the excitation energies in the discretized phonon continuum strongly depend on the box size L , this dependence disappears for the excited state below the continuum threshold. The value of α where the bound state emerges was found by repeating calculations with different L at $\alpha = 1.7$ and $\alpha = 1.8$, which resulted in the consistent crossing point shown in the inset of Fig. 2. For $L = 10l_0$, the threshold was found to be $\alpha = 1.731 \pm 0.003$.

The excitation energies were found to converge more slowly in L than the ground state energy, showing that the excited states are larger in real space than the ground state. However, the excitation energies converge more quickly in the momentum cutoff k_c than the absolute energies, and $k_c \approx 4\pi/l_0$ is large enough to find accurate excitation energies in the range of α reported here. See the Supplemental Material for more details [50].

Properties of bound excited states – The properties of the eigenstates can be studied more closely by looking at the density of virtual phonons in each mode, as shown in Fig. 3. The ground state gains more phonons as the coupling strength increases, with a larger density in the lower momentum modes. The continuum threshold state $|\text{C}\rangle$ has increased phonon density only in the $k = 0$ mode, as expected.

For weak coupling, the second excited state is mostly a combination of the Fock state with one phonon in each

of the $k = \pm 2\pi/L$ modes (one of the $a = 2, b = 0$ states), and the two Fock states with one phonon, in each of those modes respectively (the $a = 1, b = \pm 1$ states). So for weak coupling the state can be approximated as $[c_1 (\hat{a}_{2\pi/L}^\dagger + \hat{a}_{-2\pi/L}^\dagger) + c_2 \hat{a}_{2\pi/L}^\dagger \hat{a}_{-2\pi/L}^\dagger] |\text{vac}\rangle$ where $|\text{vac}\rangle$ is the phonon vacuum, for some c_1 and c_2 depending on L . As the coupling strength increases, there is a larger occupation in the other modes. For $\alpha = 2$, when this state drops below the continuum to become a bound excited state, the distribution of phonons is wider than in the ground state.

Spectral weight – The spectral weight of the state $|j\rangle$ at the total momentum P from the Hamiltonian (7)

$$Z_j^{(P)} = |\langle \text{vac} | j \rangle|^2, \quad (10)$$

carries important information about the ability to detect the state in spectroscopic measurements (e.g. angle-resolved photoemission spectroscopy (ARPES) [54–57] or polaron injection spectroscopy [58–60]). Figure 4 shows the spectral weight of the three lowest states in the discretized model. While the spectral weight of the ground state decreases $\sim 1 - \alpha/2$ for small α as expected [8], the bound excited state carries a significant spectral weight ≈ 0.2 near the threshold. The spectral weight of states within the continuum ($|\text{C}\rangle$, and $|\text{B}\rangle$ for $\alpha < 1.73$) changes with box size and is expected to vanish in the limit $L \rightarrow \infty$. The spectral weight of the discrete states ($|\text{GS}\rangle$, and $|\text{B}\rangle$ for $\alpha > 1.73$) is expected to depend weakly on the discretization of the model but a full convergence study is yet to be performed.

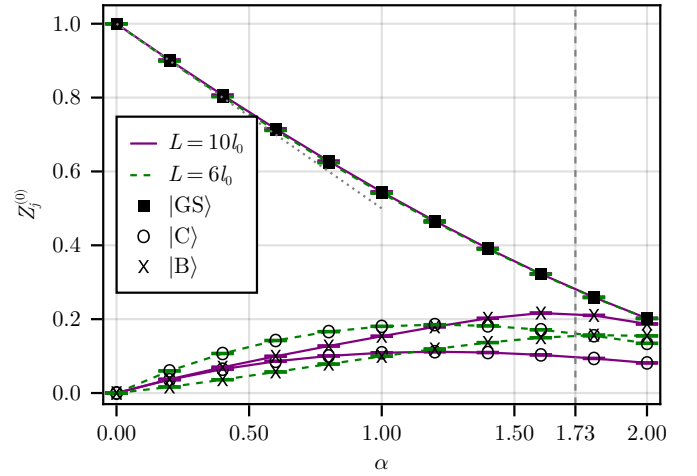


FIG. 4. Spectral weight $Z_j^{(0)}$ of the three lowest energy states vs. the coupling strength α for $k_c = 4\pi/l_0$ and two different box sizes. For $\alpha > 1.73$ marked by the vertical dashed line the state $|\text{B}\rangle$ becomes a bound excited state. The dotted line is the first order perturbation theory result $1 - \alpha/2$ for the ground state.

Outlook – An outstanding question concerns the relevance of our findings to materials [5] or experimentally accessible synthetic quantum systems [61, 62]. The closest related candidate systems may be narrow quantum wires with strong surface optical phonons [63]. Recently predicted discrete ex-

cited phonon branches near a Mott-insulator–superfluid phase transition in a Bose-Hubbard model [64] may be a related phenomenon to the excited states studied in this work. An interesting avenue of future research will be to extend the FCIQMC approach to the three-dimensional Fröhlich model to find the threshold coupling constant for the bound excited state and independently check the diagrammatic Monte Carlo results of Ref. [8], which indicated the absence of bound excited states up to values of $\alpha \approx 8$. It will further be valuable to understand the class of problems in which the resource requirements for sign-problem amelioration by walker annihilation in projector quantum Monte Carlo decouple from the dimension of Hilbert space.

Acknowledgements – We are grateful to Dmytro Kolisnyk for his help in working out the spectrum of the Hessian in the End Matter. This work was supported by the Marsden Fund of New Zealand (contract no. MAU2007) from government funding administered by the Royal Society Te Apārangi and by a summer scholarship from Te Whai Ao – Dodd-Walls Centre for Photonic and Quantum Technologies and the Physics Department, University of Auckland. We acknowledge support by the New Zealand eScience Infrastructure (NeSI) high-performance computing facilities in the form of a merit project allocation.

Data availability – All numerical calculations were performed using the open source software Rimu.jl [27]. The data that support the findings of this article are openly available [65].

* j.brand@massey.ac.nz

- [1] L. D. Landau, Über die Bewegung der Elektronen im Kristallgitter, *Phys. Z. Sowjetunion* **3**, 664 (1933).
- [2] S. I. Pekar, *Untersuchungen über die Elektronentheorie der Kristalle* (Akademie Verlag, Berlin, 1954).
- [3] H. Fröhlich, Electrons in lattice fields, *Advances in Physics* **3**, 325 (1954).
- [4] J. T. Devreese and A. S. Alexandrov, Fröhlich polaron and bipolaron: recent developments, *Reports on Progress in Physics* **72**, 066501 (2009).
- [5] C. Franchini, M. Reticcioli, M. Setvin, and U. Diebold, Polarons in materials, *Nature Reviews Materials* **6**, 560 (2021).
- [6] R. P. Feynman, Slow electrons in a polar crystal, *Physical Review* **97**, 660 (1955).
- [7] N. V. Prokof'ev and B. V. Svistunov, Polaron problem by diagrammatic quantum Monte Carlo, *Phys. Rev. Lett.* **81**, 2514 (1998).
- [8] A. S. Mishchenko, N. V. Prokof'ev, A. Sakamoto, and B. V. Svistunov, Diagrammatic quantum Monte Carlo study of the Fröhlich polaron, *Phys. Rev. B* **62**, 6317 (2000).
- [9] J. T. Titantah, C. Pierleoni, and S. Ciuchi, Free Energy of the Fröhlich Polaron in Two and Three Dimensions, *Physical Review Letters* **87**, 206406 (2001).
- [10] T. Hahn, S. Klimin, J. Tempere, J. T. Devreese, and C. Franchini, Diagrammatic Monte Carlo study of Fröhlich polaron dispersion in two and three dimensions, *Phys. Rev. B* **97**, 134305 (2018).
- [11] D. Mitrouskas and R. Seiringer, Ubiquity of bound states for the strongly coupled polaron, *Pure and Applied Analysis* **5**, 973 (2023).
- [12] J. Devreese and R. Evrard, On the excited states of a symmetrical polaron model, *Physics Letters* **11**, 278 (1964).
- [13] R. Evrard, On the excited states of the polaron, *Physics Letters* **14**, 295 (1965).
- [14] H. Sumi, Exciton Polarons of Molecular Crystal Model. I. — Dynamical CPA—, *Journal of the Physical Society of Japan* **36**, 770 (1974).
- [15] J. Bonča, S. A. Trugman, and I. Batistić, Holstein polaron, *Physical Review B* **60**, 1633 (1999).
- [16] G. L. Goodvin, M. Berciu, and G. A. Sawatzky, Green's function of the Holstein polaron, *Physical Review B* **74**, 245104 (2006).
- [17] G. H. Booth, A. J. W. Thom, and A. Alavi, Fermion Monte Carlo without fixed nodes: A game of life, death, and annihilation in Slater determinant space, *The Journal of Chemical Physics* **131**, 054106 (2009).
- [18] F. R. Petruzielo, A. A. Holmes, H. J. Changlani, M. P. Nightingale, and C. J. Umrigar, Semistochastic projector Monte Carlo method, *Physical Review Letters* **109**, 230201 (2012).
- [19] N. S. Blunt, S. D. Smart, G. H. Booth, and A. Alavi, An excited-state approach within full configuration interaction quantum Monte Carlo, *The Journal of Chemical Physics* **143**, 134117 (2015).
- [20] M. H. Kalos and P. A. Whitlock, *Monte Carlo Methods* (Wiley-VCH Verlag GmbH & Co. KGaA, Weinheim, Germany, 2008).
- [21] M. Yang, E. Pahl, and J. Brand, Improved walker population control for full configuration interaction quantum Monte Carlo, *The Journal of Chemical Physics* **153**, 174103 (2020).
- [22] J. Brand, M. Yang, and E. Pahl, Stochastic differential equation approach to understanding the population control bias in full configuration interaction quantum Monte Carlo, *Phys. Rev. B* **105**, 235144 (2022).
- [23] R. J. Anderson, C. J. C. Scott, and G. H. Booth, Full configuration interaction quantum Monte Carlo for coupled electron-boson systems and infinite spaces, *Phys. Rev. B* **106**, 155158 (2022).
- [24] S. M. Greene, R. J. Webber, T. C. Berkelbach, and J. Weare, Approximating Matrix Eigenvalues by Subspace Iteration with Repeated Random Sparsification, *SIAM Journal on Scientific Computing* **44**, A3067 (2022).
- [25] N. S. Blunt, S. D. Smart, J. A. F. Kersten, J. S. Spencer, G. H. Booth, and A. Alavi, Semi-stochastic full configuration interaction quantum Monte Carlo: Developments and application, *The Journal of Chemical Physics* **142**, 184107 (2015).
- [26] M. Čufar, C. Bradley, R. Yang, E. Pahl, and J. Brand, Rimu.jl: Random integrators for many-body quantum systems (2025), to be published.
- [27] Rimu.jl software, <https://github.com/RimuQMC/Rimu.jl>.
- [28] J. S. Spencer, N. S. Blunt, and W. M. Foulkes, The sign problem and population dynamics in the full configuration interaction quantum Monte Carlo method, *The Journal of Chemical Physics* **136**, 054110 (2012).
- [29] J. J. Shepherd, G. E. Scuseria, and J. S. Spencer, Sign problem in full configuration interaction quantum Monte Carlo: Linear and sublinear representation regimes for the exact wave function, *Physical Review B* **90**, 155130 (2014), arXiv:1407.4800v1.
- [30] A. A. Kunitsa and S. Hirata, Grid-based diffusion Monte Carlo for fermions without the fixed-node approximation, *Physical Review E* **101**, 013311 (2020).

[31] N. Liebermann, K. Ghanem, and A. Alavi, Importance-sampling FCIQMC: Solving weak sign-problem systems, *The Journal of Chemical Physics* **10.1063/5.0107317** (2022).

[32] F. M. Peeters, W. Xiaoguang, and J. T. Devreese, Ground-state energy of a polaron in n dimensions, *Phys. Rev. B* **33**, 3926 (1986).

[33] F. M. Peeters and M. A. Smondyrev, Exact and approximate results for the polaron in one dimension, *Phys. Rev. B* **43**, 4920 (1991).

[34] H. Spohn, The polaron at large total momentum, *J. Phys. A* **21**, 1199 (1988).

[35] J. S. Møller, The polaron revisited, *Reviews in Mathematical Physics* **18**, 485 (2006).

[36] R. Seiringer, Absence of excited eigenvalues for Fröhlich type polaron models at weak coupling, *Journal of Spectral Theory* **13**, 1045 (2023).

[37] J. Adamowski, B. Gerlach, and H. Leschke, Strong-coupling limit of polaron energy, revisited, *Physics Letters A* **79**, 249 (1980).

[38] M. D. Donsker and S. R. S. Varadhan, Asymptotics for the polaron, *Comm. Pure Appl. Math.* **36**, 505 (1983).

[39] E. H. Lieb and L. E. Thomas, Exact ground state energy of the strong-coupling polaron, *Comm. Math. Phys.* **183**, 511 (1997).

[40] S. Tjablikow, Adiabatische Form der Störungstheorie im Problem der Wechselwirkung eines Teilchens mit einem gequartelten Feld, *Abhandl. Sowj. Phys.* **4**, 54 (1954).

[41] G. Allcock, On the polaron rest energy and effective mass, *Advances in Physics* **5**, 412 (1956).

[42] G. Allcock, Strong-coupling theory of the polaron, in: Kuper, C.G., Whitfield, G.D. (eds.) *Polarons and Excitons*, 45 (1963).

[43] R. L. Frank and R. Seiringer, Quantum corrections to the Pekar asymptotics of a strongly coupled polaron, *Comm. Pure Appl. Math.* **74**, 544 (2021).

[44] M. Brooks and R. Seiringer, The Fröhlich polaron at strong coupling: Part I—The quantum correction to the classical energy, *Comm. Math. Phys.* **404**, 287 (2023).

[45] T. D. Lee, F. E. Low, and D. Pines, The motion of slow electrons in a polar crystal, *Phys. Rev.* **90**, 297 (1953).

[46] L.-H. Lim and J. Weare, Fast Randomized Iteration: Diffusion Monte Carlo through the Lens of Numerical Linear Algebra, *SIAM Review* **59**, 547 (2017), arXiv:1508.06104.

[47] J. J. Shepherd, L. R. Schwarz, R. E. Thomas, G. H. Booth, D. Frenkel, and A. Alavi, Emergence of Critical Phenomena in Full Configuration Interaction Quantum Monte Carlo (2012), arXiv:1209.4023.

[48] C. J. Umrigar, M. P. Nightingale, and K. J. Runge, A diffusion Monte Carlo algorithm with very small time-step errors, *The Journal of Chemical Physics* **99**, 2865 (1993).

[49] K. Ghanem, N. Liebermann, and A. Alavi, Population control bias and importance sampling in full configuration interaction quantum Monte Carlo, *Physical Review B* **103**, 155135 (2021), arXiv:2102.11016.

[50] See Supplemental Material [URL will be inserted by publisher] for numerical convergence data.

[51] Q. Chen, K. Wang, and S. Wan, An extensive calculation of the properties of a one-dimensional polaron, *Journal of Physics: Condensed Matter* **6**, 6599 (1994).

[52] M. H. Degani, O. Hipolito, R. Lobo, and G. A. Farias, Polarons in one-dimensional systems, *Journal of Physics C: Solid State Physics* **19**, 2919 (1986).

[53] B. Gerlach and H. Löwen, Analytical properties of polaron systems or: Do polaronic phase transitions exist or not?, *Reviews of Modern Physics* **63**, 63 (1991).

[54] C. N. Berglund and W. E. Spicer, Photoemission Studies of Copper and Silver: Experiment, *Physical Review* **136**, A1044 (1964).

[55] R. Y. Koyama and N. V. Smith, Photoemission Properties of Simple Metals, *Physical Review B* **2**, 3049 (1970).

[56] A. S. Mishchenko, G. De Filippis, V. Cataudella, N. Nagaosa, and H. Fehske, Optical signatures of exciton polarons from diagrammatic Monte Carlo, *Physical Review B* **97**, 045141 (2018).

[57] J. P. Nery, P. B. Allen, G. Antonius, L. Reining, A. Miglio, and X. Gonze, Quasiparticles and phonon satellites in spectral functions of semiconductors and insulators: Cumulants applied to the full first-principles theory and the Fröhlich polaron, *Physical Review B* **97**, 115145 (2018).

[58] N. B. Jørgensen, L. Wacker, K. T. Skalmstang, M. M. Parish, J. Levinsen, R. S. Christensen, G. M. Bruun, and J. J. Arlt, Observation of Attractive and Repulsive Polarons in a Bose-Einstein Condensate, *Physical Review Letters* **117**, 055302 (2016).

[59] M.-G. Hu, M. J. Van de Graaff, D. Kedar, J. P. Corson, E. A. Cornell, and D. S. Jin, Bose Polarons in the Strongly Interacting Regime, *Physical Review Letters* **117**, 055301 (2016).

[60] C. J. Vale and M. Zwierlein, Spectroscopic probes of quantum gases, *Nature Physics* **17**, 1305 (2021).

[61] P. Massignan, R. Schmidt, G. E. Astrakharchik, A. İmamoglu, M. Zwierlein, J. J. Arlt, and G. M. Bruun, *Polarons in atomic gases and two-dimensional semiconductors* (2025), arXiv:2501.09618 [cond-mat].

[62] F. Grusdt, N. Mostaan, E. Demler, and L. A. P. Ardila, *Impurities and polarons in bosonic quantum gases: A review on recent progress* (2024), arXiv:2410.09413.

[63] A. Y. Maslov and O. V. Proshina, Interface Phonons and Polaron Effect in Quantum Wires, *Nanoscale Research Letters* **5**, 1744 (2010).

[64] R. Alhyder, V. E. Colussi, M. Čufar, J. Brand, A. Recati, and G. M. Bruun, *Lattice Bose polarons at strong coupling and quantum criticality* (2024), arXiv:2412.07597.

[65] Example scripts and processed data are available on Zenodo [URL will be inserted after review]. (2025).

[66] A. Erdélyi, W. Magnus, F. Oberhettinger, and F. G. Tricomi, *Higher transcendental functions. Vol. I* (Robert E. Krieger Publishing Co., Inc., Melbourne, FL, 1981) p. 170.

[67] Specifically, all matrix elements of the operator $1 - d\tau(\hat{H}_{LLP} - S)$ that defines the FCIQMC algorithm are non-negative for small enough $d\tau$, and a ground state vector with a uniform sign is obtained upon iteration.

[68] P. J. Reynolds, D. M. Ceperley, B. J. Alder, and W. A. Lester, Jr., Fixed-node quantum Monte Carlo for molecules, *The Journal of Chemical Physics* **77**, 5593 (1982).

[69] S. Zhang, J. Carlson, and J. E. Gubernatis, Constrained path Monte Carlo method for fermion ground states, *Physical Review B* **55**, 7464 (1997).

[70] S. Zhang and H. Krakauer, Quantum Monte Carlo Method using Phase-Free Random Walks with Slater Determinants, *Physical Review Letters* **90**, 136401 (2003).

[71] D. Cleland, G. H. Booth, and A. Alavi, Communications: Survival of the fittest: Accelerating convergence in full configuration-interaction quantum Monte Carlo., *The Journal of chemical physics* **132**, 041103 (2010).

END MATTER

Appendix A: Eigenvalues of the Hessian of the Pekar functional – Here we shall justify Eq. (5) for the Hessian of the Pekar functional, as well as the stated values for the eigen-frequencies ω_j . Since $\min_{\psi} \mathcal{E}^P(\psi, \varphi)$ is equal to the sum of $\int |\varphi|^2$ and the ground state energy of the effective Hamiltonian $-\partial^2 - 2\sqrt{2\alpha} \operatorname{Re}(\varphi)$, simple second order perturbation theory leads to

$$\hat{\omega}^2 = 1 - 8\alpha\psi^P \frac{Q}{-\partial^2 - 2\sqrt{2\alpha}\varphi^P + \alpha^2} \psi^P \quad (\text{A1})$$

where Q projects orthogonal to ψ^P . Note that ψ^P is the zero-energy ground state of $-\partial^2 - 2\sqrt{2\alpha}\varphi^P + \alpha^2 = A^\dagger A$ with $A = \partial - (\psi^P)/\psi^P$. We can write $(A^\dagger A)^{-1}Q = A^\dagger(AA^\dagger)^{-2}A$. Since $AA^\dagger = -\partial^2 + \alpha^2$, and $A\psi^P = \psi^P\partial$, this leads to Eq. (5) in the main text.

The eigenvalue equation $\hat{\omega}^2 f = \omega^2 f$ can be rewritten in terms of λ defined by $\omega^2 \equiv 1 - \lambda$ as

$$\left(\partial^2 - 4\frac{(\psi^P)'}{\psi^P}\partial + 4\alpha^2 + \frac{8\alpha}{\lambda}(\psi^P)^2 \right) f' = 0 \quad (\text{A2})$$

This follows from the identity $\psi^P(-\partial^2 + \alpha^2)^2(\psi^P)^{-1} = (\partial^2 - 4\frac{(\psi^P)'}{\psi^P}\partial + 4\alpha^2)\partial^2$. Changing variables from x to $t = -\alpha^{-1}\psi^P(x)/\psi^P(x) = \tanh(\alpha x)$ and making the ansatz $f'(x) = \ell(t)(1-t^2)$ turns Eq. (A2) into the standard Legendre equation

$$(1-t^2)\ell'' - 2t\ell' + n(n+1)\ell = 0 \quad (\text{A3})$$

with $n(n+1) = 2 + 4\lambda^{-1}$. The general solution is thus a linear combination of L_n^P and L_n^Q , the Legendre functions. The condition that the resulting function f be square-integrable introduces the constraints $\int_{-1}^1 \ell(t)dt = 0$ and $\int_{-1}^1 \ell(t) \ln \frac{1+t}{1-t} dt = 0$ or, equivalently, $\int_{-1}^1 \ell(t)L_0^P(t)dt = 0 = \int_{-1}^1 \ell(t)L_0^Q(t)dt$ (due to the fact that $\int_{-\infty}^{\infty} f'(x)dx = 0$ and also $\int_{-\infty}^{\infty} f(x)dx = 0$ since f itself is a derivative).

The even solutions of Eq. (A3), satisfying the orthogonality constraints, are simply the Legendre polynomials L_n^P for $n = 2, 4, 6, \dots$. This leads to (with $j \equiv n-2$)

$$\omega_j^2 = 1 - \frac{4}{(j+4)(j+1)}, \quad j = 0, 2, 4, \dots \quad (\text{A4})$$

In particular, $\omega_0 = 0$ and $\omega_2 = \sqrt{7/9}$. The odd solutions are slightly more complicated. They are linear combinations of L_n^P and L_n^Q for non-integer n . Using the well-known integrals over products of Legendre functions in [66], the orthogonality conditions transform to the equation

$$\psi_{\Gamma}(n+1) + \gamma = \frac{\pi}{2} \tan \frac{n\pi}{2} \quad (\text{A5})$$

where $\psi_{\Gamma} = \Gamma'/\Gamma$ denotes the digamma function, and $\gamma \approx 0.577$ is Euler's constant. There are infinitely many solutions,

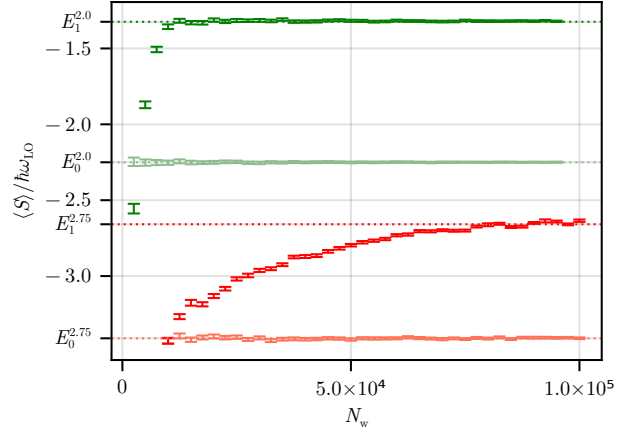


FIG. 5. Overcoming the sign problem by walker annihilation. The mean of the shift energy $\langle S \rangle$ is shown as a function of the number of walkers N_w for the ground and first excited states at two values of the interaction strength $\alpha = 2.0$ (green) and $\alpha = 2.75$ (red), with $L = 6l_0$ and $k_c = 4\pi/l_0$. The critical number of walkers N_c above which the mean shift becomes an estimator for the excited state energy depends on the interaction strength α .

one in every interval $(2j, 2j+1)$ for $j \geq 1$, the smallest being $n_1 \approx 2.523$. Denoting the solution in the interval $(2j, 2j+1)$ by n_{2j-1} , we thus conclude that

$$\omega_j^2 = 1 - \frac{4}{(n_j+2)(n_j-1)}, \quad j = 1, 3, 5, \dots \quad (\text{A6})$$

In particular, $\omega_1 \approx 0.647$.

Appendix B: Overcoming the sign problem in excited state FCIQMC – The Hamiltonian of the Fröhlich polaron of Eq. (7) is stoquastic, i.e. all non-zero off-diagonal elements are negative. Thus, it avoids the sign problem for the ground state, as stochastic spawns never change the sign of a walker [67]. This changes for the calculation of excited states where the Gram-Schmidt projector introduces sign-changing contributions to coefficients. In the absence of walker annihilation or at a small number of walkers where annihilation is inefficient, the iterations converge to a ground state of a different Hamiltonian with a lower (incorrect) ground state energy [28]. This leads to an incorrect value of the mean shift energy $\langle S \rangle$. Typically, the presence of a sign problem in Projector Monte Carlo requires a suppression mechanism that introduces uncontrolled approximations (e.g. fixed nodes [68], a constrained path [69], the phaseless [70] or initiator method [71]). Formulated in a discrete Hilbert space, FCIQMC can overcome the sign problem by walker annihilation, avoiding such approximations, if the coefficient vector is sufficiently strongly localized [17, 28, 29].

Figure 5 shows how the mean shift energy depends on the number of walkers for the ground and the first excited state of the Fröhlich polaron problem. For the ground state, the mean shift only carries small stochastic fluctuations and is a valid estimator for the ground state energy regardless of the walker number because the sign problem is absent. The population control bias, which raises $\langle S \rangle$ above the correct value for small walker numbers [22], is smaller than the stochastic errors in this case. For the excited states, the strong dependence of the shift energy on the walker number below a critical

value indicates the presence of a sign problem. Above the critical walker number N_c , the mean of the shift fluctuates around the correct value of the excited state energy. This critical number is found to be strongly dependent on the value of the coupling strength α . We find values of around $N_c \approx 1 \times 10^4$ for $\alpha = 2.0$ and $N_c \approx 1 \times 10^5$ for $\alpha = 2.75$, as seen from Fig. 5. The calculations reported in Figs. 2, 3 and 4 were obtained with N_w on the order of 10^6 or 10^7 , at least an order of magnitude higher than the observed critical values N_c for overcoming the sign problem.

Supplemental Material: Bound excited states of Fröhlich polarons in one dimension

J. Taylor,^{1,2,3,4} M. Čufar,^{1,2} D. Mitrouskas,⁵ R. Seiringer,⁵ E. Pahl,^{3,4} and J. Brand^{1,2,*}

¹Dodd-Walls Centre for Photonic and Quantum Technologies, Auckland 0745, New Zealand

²Centre for Theoretical Chemistry and Physics, New Zealand Institute for Advanced Study, Massey University, Private Bag 102904, North Shore, Auckland 0745, New Zealand

³MacDiarmid Institute for Advanced Materials and Nanotechnology, Auckland 1010, New Zealand

⁴Department of Physics, University of Auckland, Auckland 1010, New Zealand

⁵Institute of Science and Technology Austria (ISTA), Am Campus 1, 3400 Klosterneuburg, Austria

(Dated: June 3, 2025)

GROUND STATE ENERGY CONVERGENCE

The energy of the ground state calculated using our computational model has a systematic discretization error, with the energy becoming more accurate as the box size L and the momentum cutoff k_c are increased.

The results shown here use a coupling strength of $\alpha = 2$. For different α the overall behavior is the same, with the errors caused by finite L and k_c being roughly proportional to the ground state energy.

Keeping L constant, the ground state energy decreases with increasing momentum cutoff k_c consistent with algebraic convergence, as shown in Fig. S1. The best fit curve is

$$E_0/(\hbar\omega_{\text{LO}}) = -2.3455 \pm 0.0039 + \left[(0.4110 \pm 0.0070) \frac{k_c l_0}{\pi} \right]^{(-1.0568 \pm 0.0451)}. \quad (\text{S1})$$

The exponent was found to be close to -1 for other values of α as well.

Using this, we can estimate that the error incurred in the ground state energy from limiting the maximum phonon wavenumber to $k_c = 12\pi/l_0$ is $(0.0297 \pm 0.0064)\hbar\omega_{\text{LO}}$, about 1.3% of the energy. For $k_c = 4\pi/l_0$ the error is $(0.095 \pm 0.0082)\hbar\omega_{\text{LO}}$, about 4.1% of the energy.

Figure S2 suggests an exponential convergence of the energy in the box size L when k_c is kept constant. The best fit curve is

$$E_0/(\hbar\omega_{\text{LO}}) = -2.3089 \pm 0.0008 - (9.5077 \pm 0.2381) \exp \left[-(1.5976 \pm 0.0132) \frac{L}{l_0} \right]. \quad (\text{S2})$$

Note that the value at infinite L is too high since the momentum cutoff is finite. The error caused by the finite box size at $L = 6l_0$ can be estimated from the observed exponential convergence to be $(0.00065 \pm 0.0011)\hbar\omega_{\text{LO}}$, consistent with no error.

The calculations reported in Fig. 1 in the main text were performed at $L = 6l_0$ and $k_c = 12\pi/l_0$. These calculations with $M = 73$ modes used 2×10^5 walkers to probe a Hilbert space with dimension $256^M \approx 6 \times 10^{175}$. The number of non-zero vector coefficients was strongly dependent on α . For $\alpha =$

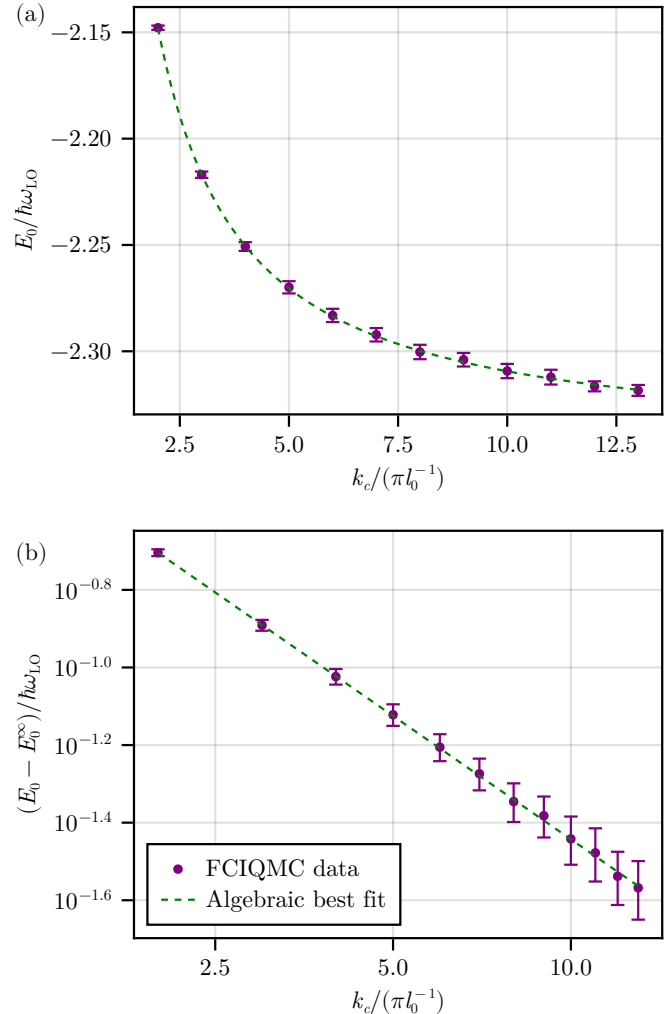


FIG. S1. (a) The ground state energy for $\alpha = 2$ with $L = 6l_0$ as a function of the cutoff k_c . (b) The difference between the ground state energy and the extrapolated energy at infinite k_c , on a log-log plot. The trend suggests an algebraic convergence of the energy, with an error in the energy proportional to approximately k_c^{-1} .

0.25 there were about 1.4×10^4 non-zero coefficients, whereas for $\alpha = 2$ there were about 1.8×10^5 , almost as many as the number of walkers. Evolving for about 10^6 steps resulted in a stochastic error in the energy estimate of approximately $3 \times 10^{-3}\hbar\omega_{\text{LO}}$ for $\alpha = 2$. This is an order of magnitude

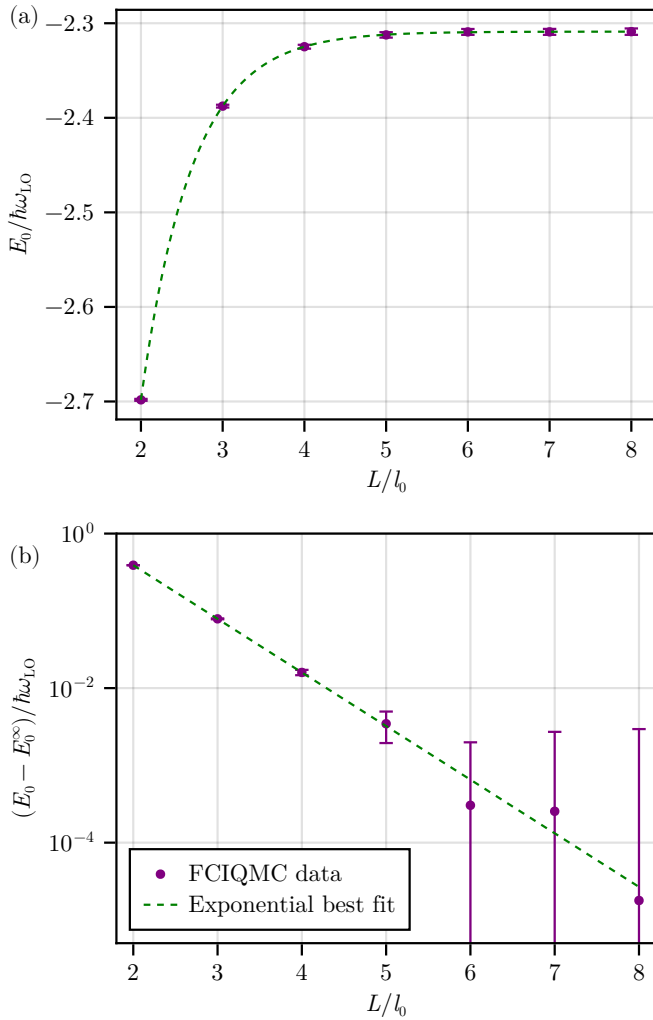


FIG. S2. (a) The ground state energy for $\alpha = 2$ with $k_c = 10\pi/l_0$, for various box sizes L . (b) The difference between the ground state energy and the extrapolated energy at infinite L , on a semi-log plot. In this case, the data imply an exponential convergence of the energy.

smaller than the estimated discretization error due to the finite value of k_c .

BOUND EXCITED STATE

At $\alpha = 2$, the first excited state is discrete corresponding to an excitation of the phonon cloud that is bound to the electron (polaron). The energy of this state converges in k_c in a similar way to the ground state indicating algebraic convergence. See Fig. S3(a). The best fit curve (at $L = 6l_0$) is

$$E_1/(\hbar\omega_{\text{LO}}) = -1.4082 \pm 0.0046 + \left[(0.4429 \pm 0.0046) \frac{k_c l_0}{\pi} \right]^{-1.2002 \pm 0.0576}. \quad (\text{S3})$$

Although the excited state energy has a similarly slow convergence with k_c as the ground state, we find that the differ-

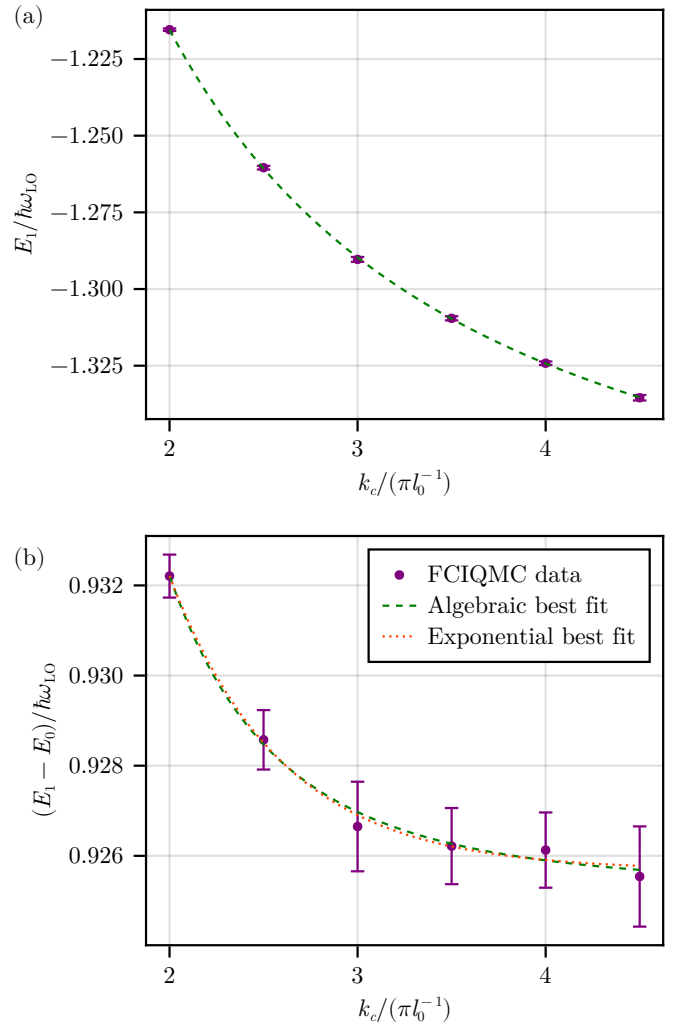


FIG. S3. (a) Energy of the first excited state for $\alpha = 2$ and $L = 6l_0$, with varying momentum cutoff. There is an apparent algebraic convergence, similar to that of the ground state energy. (b) The energy difference between the bound excited state and the ground state for $\alpha = 2$ and $L = 6l_0$, with varying k_c . The energy difference converges more quickly than the energies of the states separately.

ence between the two, i.e. the excitation energy, converges much more quickly in k_c , see Fig. S3(b). Therefore, even though there is a large error in the energies of the ground state and first excited state separately with a momentum cutoff of $k_c = 4\pi/l_0$, this k_c is large enough to find the excitation energy. With a momentum cutoff this small, the energies of the ground state and the excited states are too high by about $0.1\hbar\omega_{\text{LO}}$, but the differences between the states are constrained mostly to the low momentum modes resulting in more precise excitation energies. While the numerical data is not accurate enough to distinguish between algebraic and exponential convergence, both extrapolations estimate a systematic error at $k_c = 4\pi/l_0$ that is smaller than the stochastic error bar and consistent with no error.

On the other hand, Fig. S4 shows that the energy of the first excited state converges more slowly in L than the ground

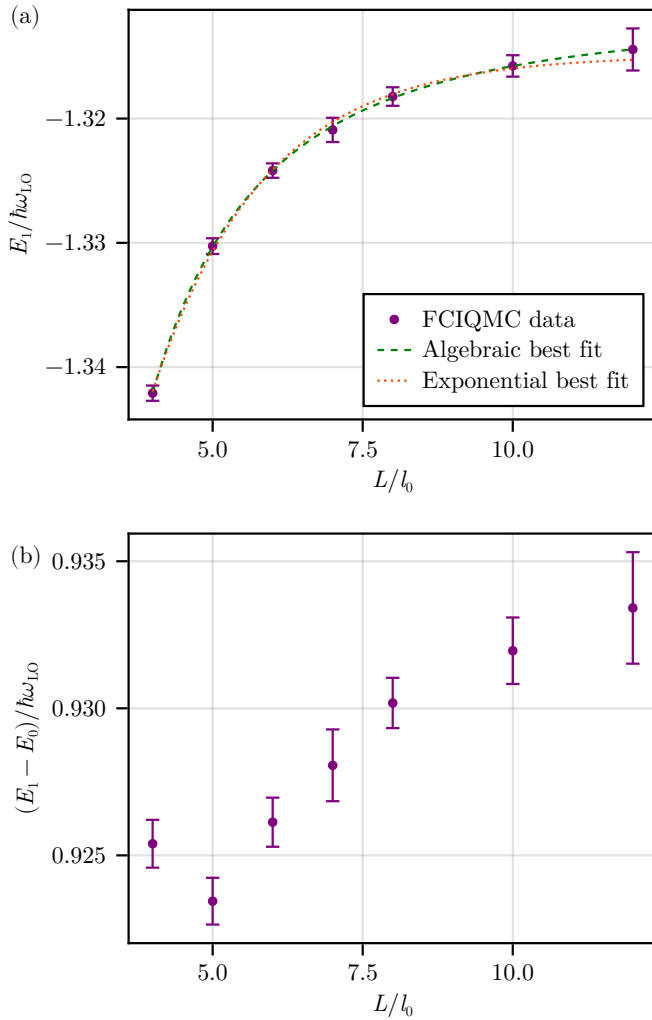


FIG. S4. (a) Energy of the first excited state for $\alpha = 2$ and $k_c = 4\pi/l_0$, with varying box size. The rate of convergence is unclear, but even with a slow algebraic convergence the box size error is on the order of $0.01\hbar\omega_{\text{LO}}$. (b) The excitation energy of the bound state with the same parameters. This is not monotonic because the energies of the two states converge differently.

state, which was already converged at $L = 6l_0$. With an exponential fit, the exponent is $(-0.54 \pm 0.05)L/l_0$, indicating a slower convergence than the ground state (S2).

Assuming instead an algebraic convergence for the worst case scenario, the error in the excitation energy caused by the finite box size at $L = 6l_0$ estimated from extrapolation is $(0.0100 \pm 0.0018)\hbar\omega_{\text{LO}}$.

CONTINUUM EXCITED STATES

The excited states we find in the continuum have excitation energies larger than $1\hbar\omega_{\text{LO}}$ with a $1/L$ energy dependence only because our computational model is discretized. In the limit $L \rightarrow \infty$, all excitation energies of the individual discrete states shown in Fig. 2 of the main paper would converge to $1\hbar\omega_{\text{LO}}$. Note that this means that the linear interpolation used to find the crossover point for the bound excited state (see Figure 2 in main paper) is only valid up to a certain precision. To find the crossing point more precisely with large L , one would need to take more data at smaller intervals of α .

* j.brand@massey.ac.nz